Physical analysis and modeling of the Falcon concentrator for beneficiation of ultrafine particles

Jean-Sébastien Kroll-Rabotin[a,c], Florent Bourgeois[a,c,*], Éric Climent[b,c]

[a] *University of Toulouse, INPT-UPS-CNRS: Laboratoire de Génie Chimique, Toulouse, France*
[b] *University of Toulouse, INPT-UPS-CNRS: Institut de Mécanique des Fluides, Toulouse, France*
[c] *Fédération de recherche FERMaT, CNRS FR 3089 - Toulouse, France*

Abstract

A predictive model of the Falcon enhanced gravity separator has been derived from a physical analysis of its separation principle, and validated against experimental data. After summarizing the previous works that led to this model and the hypotheses on which they rely, the model is extended to cover a wide range of operating conditions and particle properties. The most significant development presented here is the extension of the analytical law to concentrated suspensions, which makes it applicable to actual plant operating conditions. Two examples of industrial use cases are described and studied by interrogation of the model: dredged sediment waste reduction and coal recovery from fine tailings. Comparisons with empirical studies available in the literature show a good agreement between model predictions and industrial data. The model is then used to identify separation efficiency limitations as well as possible solutions to overcome them. These two examples serve to show how this predictive model can be used to obtain valuable information to improve physical separation processes using a Falcon concentrator, or to evaluate Falcon separator's abilities for new applications.

Keywords: Gravity concentration, Physical separation, Modeling, Fine particle beneficiation

Introduction

Falcon concentrators are enhanced gravity separators (EGS) consisting of a fast spinning bowl. The bowl is fed from its bottom and uses centrifugal force to drain the slurry in a thin flowing film at its wall. During operation, part of the transported particles is retained inside the bowl, while the other part flows out with the fluid. Due to high rotation rate, the centrifugal force in the flowing film can be several orders of magnitude greater than Earth' attraction. Different mechanisms have been identified as playing significant roles in the separation taking place inside the bowl (Abela, 1997; Deveau, 2006; Laplante et al., 1994; Laplante and Nickoletopoulos, 1997; Laplante and Shu, 1993; McAlister and Armstrong, 1998), such as particle differential settling in the bottom region of the bowl, near the film inlet (Zhao et al., 2006).

Three bowl series differ by the way they trap particles once particles have been classified by differential settling in the flowing film. Falcon SB series uses fluidized annular grooves upstream of the bowl outlet. The retention capacity of the bowl can thus be set by adjusting the counter-pressure flow rate. Falcon UF series uses smooth bowls with a slight reduction in diameter at the outlet. This lip creates a non-flowing region whose volume varies with the bowl's opening angle (Holtham et al., 2005). In this case, the film flows over a retention zone that has no fluidization counter-pressure. Both series are essentially semi-batch: "heavy" particles are recovered by interrupting operation and emptying the retention zone before a new operating cycle starts. The third design — C series — operates similarly to the UF series, but adds a slot in the retention zone that is equipped with discharge valves with variable size apertures. In this way, the discharge rate in the retention zone can be adjusted, which makes it possible to operate the bowl continuously (Abela, 1997; Honaker et al., 1996; McAlister and Armstrong, 1998).

Commercial brochures published by Falcon indicate recovery abilities for C and UF series down to 10 and 3 μm respectively for targeted applications to heavy materials (tin, tantalum, tungsten, chrome, cobalt and iron). The UF series are more limited in terms of capacity (up to 20 m^3/h for the bigger bowls) due to their design oriented towards ultrafine particle recovery. This study focuses on these concentrator series because of their potential application to fine dredged sediments. Nevertheless, a number of conclusions drawn from physical analysis of these concentrators remain valid for other series.

1. Separation modeling

1.1. Physical analysis and hypotheses

The assumptions on which our modeling of the smooth-wall Falcon device relies, have already been described in previous publications (Kroll-Rabotin, 2010; Kroll-Rabotin et al., 2010,

*Corresponding author
Email addresses: jean-sebastien.kroll-rabotin@ualberta.ca (Jean-Sébastien Kroll-Rabotin), florent.bourgeois@ensiacet.fr (Florent Bourgeois), climent@imft.fr (Éric Climent)

2011a,b). The fundamental hypothesis on which our modeling is based is that once particles enter the bowl retention zone, they never leave it. Moreover, any classification upstream of the flowing film is neglected: it is assumed that the impeller at the bottom of the bowl plays no active role in the separation — ot is considered in fact that it homogenizes the feed that enters the flowing film. Suspension is then considered homogeneous at the film inlet which implies that the prevalent separation mechanism is particle transport in the flowing film before particles reach the retention zone or the bowl outlet. Our predictive model was then built by solving a simplified particle transport equation analytically.

The evolution of the flowing film thickness along the bowl wall is neglected, so that the flow is modeled by the combination of a semi-parabolic profile in the streamwise direction and a solid body rotation. This simplification is discussed in section §1.2.

Once the flow has been modeled, a transport model is added to it in order to predict separation. To achieve this, numerical and analytical solutions of Lagrangian (Kroll-Rabotin et al., 2010), and Eulerian tracking of particles in the film were obtained (Kroll-Rabotin et al., 2011a).

The analytical solution is obtained by neglecting particle interactions. Therefore, it is only reliable to predict separation in dilute suspensions. Particle transport is then governed by the balance between drag and centrifugal forces acting on particles. For this balance to be sufficient to account for the real physics, particle inertia must be neglected. Also, in order to get an analytical solution, the drag law must remain linear. These two assumptions limit analytical predictions to low Stokes and low particulate Reynolds numbers. However, it is shown in section 2.2 that it does not affect the accuracy of the model.

Finally, the recovery of a given particle type — characterized by its radius (r_p) and density (ρ_p) — in a smooth wall Falcon bowl is given by:

$$C_p = \min\left(\frac{4\pi}{9}\,\lambda\,Q^{-1}\,\omega^2\,(\rho_p-\rho_f)\,r_p^2\,\mu^{-1}\right.$$
$$\left.R_{\min}\,R_{\max}\,H_{\text{bowl}},\quad 1\right) \tag{1a}$$

where C_p is the equation of the partition surface. In this equation Q and ω are the operating conditions (feed and bowl rotation rates), ρ_f and μ are the carrier fluid properties (density and dynamic viscosity). $R_{\min}$, $R_{\max}$ and H_{bowl} define the bowl geometry (base radius, radius at the outlet and height) and λ is a calibration constant. Experiments yielded a value of $\lambda = 0.68$ for a laboratory scale Falcon L40 equipped with a UF bowl (Kroll-Rabotin et al., 2011b). The need of a calibration constant has already been detailed extensively in Kroll-Rabotin et al. (2011b): it actually only reflects the simplifications we have included in the model derivation such as:

- bowl geometry (as it is simplified to the 3 parameters $R_{\min}$, $R_{\max}$ and H_{bowl}, while actual bowls are made of a few parts with different opening angles, include trapping mechanisms, etc);
- rotation as a solid body (which may contain up to almost 10% error as stated in section 1.2);
- other neglected terms detailed in the model derivation.

Among those three points, the first one seems to be the most significant, and is the reason why the calibration should be evaluated for each bowl shape (which differs slightly between bowl sizes and Falcon series). The fact that the calibration constant's order of magnitude is around unity confirms that it only contains corrective terms and does not hide any unaccounted significant physical phenomenon.

It is worth mentioning that due to the balance between drag and centrifugal forces, theoretical particulate Reynolds number and Archimedes number are related. For particles whose settling follows Stokes' drag law, $Re_p = (3\pi)^{-1}Ar$. Because of that, it is commonly said that particulate Reynolds number governs separation in gravity separators. This is not effectively true in this case as it does not accurately account for the effects of flow rate and particle size, as shown is this other form of equation (1a):

$$C_p = \min\left(\frac{1}{3}\,Ar\,\lambda\,Q^{-1}\,r_p^{-1}\,\nu\,R\,H_{\text{bowl}},\quad 1\right) \tag{1b}$$

In this expression, a pseudo Reynolds number appears. It is based on particle size and on velocity $Q/(RH)$ which has no direct physical meaning, since Q is the feed flow rate and $R \times H$ is half the area of the bowl azimuthal section. This simple overview of the model already shows that although such gravity concentrators are used to perform separation according to particle densities, particle size is also playing a significant role in their performances (Coulter and Subasinghe, 2005).

1.2. Modeling of the flow profile

A major difficulty in the flow field computation is the free surface of the film which yields a boundary condition whose position is unknown until the problem is fully solved. It could be solved numerically by interface tracking or with the "*Volume of Fluid*" method (Dijk et al., 2001) that solves the physics continuously between the liquid and gas phases by weighing them according to their respective local volume fractions. This method would make it possible to compute the flowing film thinning along the bowl wall. However, such an approach is only required when the film thickness undergoes significant variations. Another approach that has been described thoroughly in the literature gives analytical solutions of the simplified Navier-Stokes equations in a rotating referential (Bruin, 1969; Janse et al., 2000; Langrish et al., 2003; Makarytchev et al., 1998, 1997).

In a Falcon concentrator, the centrifugal force due to the bowl spinning reaches several hundreds of times the Earth's gravitation (from 100 to 600 G depending on the series). For high Froude numbers Makarytchev et al. (1997) give:

$$h = \left(\frac{3\nu Q}{2\pi\omega^2 r^2 \sin\frac{\beta}{2}}\right)^{1/3} \tag{2}$$

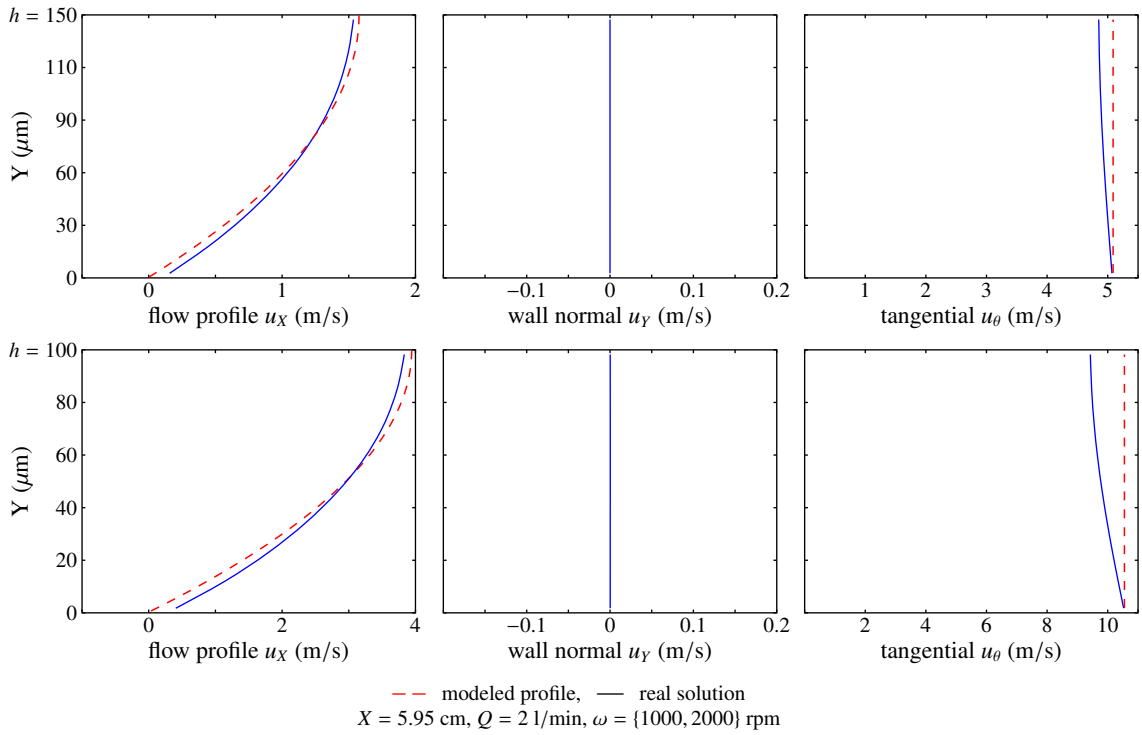

Figure 1: Comparison of modeled flow profiles with DNS solutions

This simplified law expresses how film thickness changes as a function of the operating and geometrical parameters. In particular, expression (2) yields the thickness ratio between the bottom of the bowl (h_i) and the outlet (h_f):

$$\frac{h_f}{h_i} = \left(1 + \frac{H_{\text{bowl}}}{R_0} \tan\frac{\beta}{2}\right)^{-2/3} \tag{3}$$

For a Falcon L40 with a UF bowl, this ratio is approximately 0.8 which confirms the validity of the constant thickness assumption when compared to the shape ratio of the film azimuthal section. It only depends on geometrical properties and is approximately the same for all Falcon series, even for industrial scale bowls. As a result, variations of the film thickness are neglected in our modeling.

In the streamwise direction (parallel to the bowl wall), for high Froude numbers and high rotation rates, the analytical solution given by Makarytchev et al. (1997) is a semi-parabolic profile:

$$u_X \approx \frac{Q}{2\pi r h} P\left(\frac{Y}{h}\right) \tag{4a}$$

$$P\left(\frac{Y}{h}\right) = \frac{3}{2}\left(2\frac{Y}{h} - \frac{Y^2}{h^2}\right) \tag{4b}$$

In the azimuthal plane, the only simplification that was added to the analytical solution is the constant film thickness, so wall-normal fluid velocity is neglected:

$$u_Y = 0 \tag{5}$$

The only shear source in the azimuthal direction is Coriolis acceleration. Indeed, fast rotation speed may induce significant Coriolis effects that make the flow fully three-dimensional. The azimuthal velocity profile is also given by Makarytchev et al. (1997) as:

$$u_\theta = \omega r\left(1 + \frac{1}{4} Ek^{-2} P_\theta\left(\frac{Y}{h}\right)\right) \tag{6a}$$

$$P_\theta\left(\frac{Y}{h}\right) = \left(\frac{Y}{h}\right)^3 - \frac{1}{4}\left(\frac{Y}{h}\right)^4 - 2\frac{Y}{h} \tag{6b}$$

$$Ek = \frac{\nu}{2\omega h^2 \sin\frac{\beta}{2}} \tag{6c}$$

The non-dimensional parameter Ek is not explicitly identified in the expression given by Makarytchev et al. (1997). However, expressing it explicitly makes physical interpretation easier. Ek is the Ekman number which is the ratio of viscous effects relative to Coriolis inertial force. Its expression shows that when viscous effects prevail, wall rotation propagates throughout the whole film and azimuthal velocity tends to rotation as a solid body. When Coriolis effects become more and more important, they perturb the base flow so that it looks more and more like profile P_θ. As this profile strongly depends on film thickness, using constant thickness assumption in equations (6) gives inconsistent profiles. It cannot be used when film thickness variation is not explicitly taken into account. However, direct numerical simulation (DNS) results show that the error is smaller than 10% (cf. figure 1) between rotation as a solid body and real azimuthal velocity for an opening angle of 20°. Consequently, azimuthal velocity is considered as the rotation of a solid body

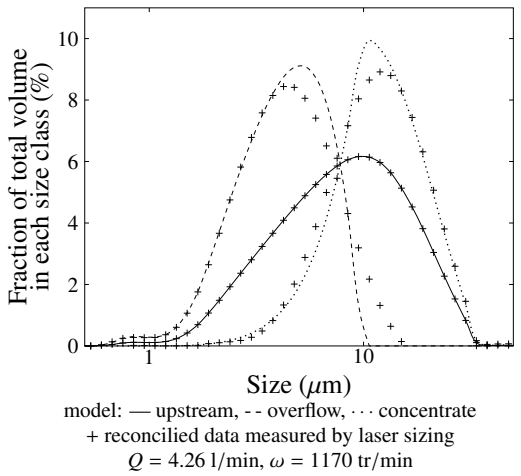

Figure 2: Comparison between measurements with a Malvern Mastersizer 2000 and model predictions

$u_\theta = \omega r$ throughout the rest of this article.

Finally, the fluid flow is modeled by combining the rotation as a solid body for u_θ with a semi-parabolic profile for u_X. This flow gives good approximation of the real flow in a fast spinning bowl with a small opening angle.

1.3. Validation of the separation model

The analytical model (1a) has been validated against experimental data (Kroll-Rabotin et al., 2011b) using a Falcon L40 equipped with a UF smooth bowl. In order to relate recovery to particle physical properties, particles with the same density were used in the experiments. Particle size distributions in the feed, concentrate and tailing streams were measured by laser diffraction sizing. This technique allowed us to determine the value of the calibration constant λ for the device and to verify the model accuracy, thus validating the aforementioned hypotheses.

Figure 2 shows all the laser sizing measurements and model predictions for a given experimental run. The data are plotted in the same manner as the sizing device provides them: one point for each measured size class (size ranges vary exponentially so that data points are regularly spaced on the semi-logarithmic scaled curve). Vertical axis directly gives the probability associated with a finite size range instead of the more usual probability density associated with a unique size. Predictions are plotted with continuous lines and expressed in the same unit.

The good agreement between experimental results and model predictions validates the model. The only noticeable difference is that measured size distributions show smoother variations than predictions in regions where predictions vary very sharply. Actually, laser sizers are known to have limited ability to track sharp variations in measured distributions. Smoothing of measurements is a laser sizing effect which by itself is enough to explain the difference between predictions and size measurements, while the whole set of other data points confirms the accuracy of the physics accounted for in equation (1a).

2. Coarse and dense particles

For a more precise consideration of the physics compared to what has been used in the model derivation, particle trajectory may be calculated based on a more comprehensive force balance at each point along the trajectory. To account for drag force, buoyancy, added mass force and the effect of pressure gradient, force balance is expressed as follows (Kroll-Rabotin et al., 2010) for the modeled velocity field described in equation (4) that satisfies $\mathrm{D}\vec{u}/\mathrm{D}t = 0$:

$$\left(\rho_p + \rho_f C_M\right) \frac{\mathrm{d}\vec{v}}{\mathrm{d}t} = \left(\rho_p - \rho_f\right) \vec{G} - \frac{3}{8\, r_p} \rho_f\, C_D\, \|\vec{v} - \vec{u}\|\, (\vec{v} - \vec{u}) \quad (7)$$

By neglecting the slip between the particles and the fluid in the azimuthal direction, equation (7) can be solved in the azimuthal plane only:

$$\left(\rho_p + \rho_f C_M\right) \frac{\mathrm{d}\vec{v}_{2\mathrm{D}}}{\mathrm{d}t} = \left(\rho_p - \rho_f\right) \left(\omega^2 r \vec{e}_r + \vec{G}\right) - \frac{3}{8\, r_p} \rho_f\, C_D\, \|\vec{v}_{2\mathrm{D}} - \vec{u}_{2\mathrm{D}}\|\, (\vec{v}_{2\mathrm{D}} - \vec{u}_{2\mathrm{D}}) \quad (8)$$

2.1. Numerical resolution of the Lagrangian tracking

To extend the scope of this modeling to dense and coarse particles, equation (8) must be solved for all Stokes and particulate Reynolds numbers. This means that particle inertia cannot be neglected, which turns the force balance used in the analytical model into a partial differential equation. It also means that drag force becomes a non linear function of the slip velocity of particles in the fluid. The expression from Schiller and Naumann (1935) is used for the drag coefficient:

$$C_D = \frac{24}{Re_p} \left(1 + 0.15 Re_p^{0.687}\right) \quad (9a)$$

$$\text{with } Re_p = 2 \frac{\|\vec{u}_{2\mathrm{D}} - \vec{v}_{2\mathrm{D}}\| r_p}{\nu} \quad (9b)$$

As there is no analytical solution for equation (8), numerical methods are required to solve this new model. The following results have been computed using an explicit time scheme solver in which fluid velocity is expressed analytically at every point using equations (4) and (5).

2.2. Physical limitations of the separation

According to the previous observations, separation based on a density criterion with a Falcon concentrator would be more efficient for high particulate Reynolds numbers (Kroll-Rabotin et al., 2010) and high Stokes numbers (Kroll-Rabotin, 2010). The analytical model is not able to take these effects into account, but in cases of low values for these numbers, for which it is accurate, it shows that the écart probable (E_p) is proportional to the difference between the cut-point density and the density of the fluid carrying the suspension. This comes from model (1a) which gives a linear relation between the recovery

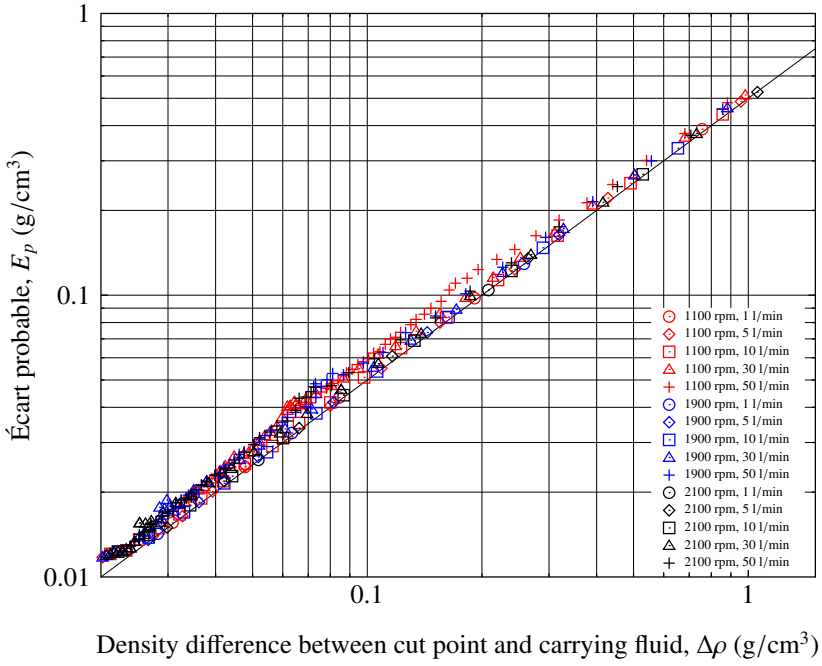

Figure 3: Relationship between the écart probable and the cut-point density for dilute suspensions

ratio and the density difference between the particles and the carrying fluid.

The analytical solution of the model relies on a few hypotheses which are only valid for low Stokes and particulate Reynolds numbers. In order to quantify the differences between the numerical solution and the analytical model in terms of predicted separation efficiency, figure 3 shows the relationship between the écart probable (E_p) and the cut-point density (ρ_{50}) obtained by numerical resolution. The analytical model always gives a value of $E_p/\rho_{50} = 0.5$ for all operating conditions. Figure 3 shows that for all operating conditions, even quite away from the actual range of operating conditions achievable by Falcon bowls, points remain aligned on the same straight line $E_p/\rho_{50} \approx 0.5$. This demonstrates that for all particle distributions that can be treated with a Falcon concentrator, there is no subset of operating conditions for which the effects of particle inertia and of non-linear drag, which have been neglected in the analytical law (1a) play a significant role. The conclusion is that in the operation conditions we consider in this paper, there is no significant error when using correlations only valid for low Stokes and particulate Reynolds numbers, so the Stokes and particulate Reynolds numbers can always be considered as low, in the sense that asymptotic behaviour for low values gives good results for all operating conditions at which Falcon concentrators operate.

This conclusion, confirmed by experimental results using a small scale Falcon device, can *a priori* be extended to all Falcon concentrator series since, for a given separation, particulate Reynolds number decreases with increasing bowl radius. Indeed, relatively low particulate Reynolds numbers (that is $Re_p \lessapprox 1$) can be estimated using the analytical expression of the forces balanced in the scaling law (Stokes drag law and centrifugal force), which yields an approximated theoretical value ($Re_{p_{\text{th}}}$) that is a good estimation of the real particulate Reynolds number:

$$Re_{p_{\text{th}}} = \frac{4}{9}\left(\frac{\rho_p}{\rho_f} - 1\right)\frac{\omega^2 r_p^3 R}{\nu^2} \tag{10}$$

Combining equations (1a) and (10), the rate of change of particulate Reynolds number with bowl size, at iso-recovery, are:

$$\frac{Re_p}{C_p} \propto \frac{\omega^2\, R}{\omega^2\, R_{\text{min}}\, R_{\text{max}}\, H_{\text{bowl}}} \approx \left(R\, H_{\text{bowl}}\right)^{-1} \tag{11}$$

Equation (11) shows that in order to achieve constant separation, increasing bowl size (radius and/or length) makes the particulate Reynolds number decrease. So, as the effect of this number is negligible on separation with a laboratory scale Falcon L40, it is also negligible for all bigger Falcon concentrators. In the expression of the particulate Reynolds number (10), the physical quantity whose exponent prevails is particle size, with a cubic law. The main input parameter that could make it possible to leverage particulate Reynolds effect on density separation efficiency is by changing the washability of the treated suspension. Unfortunately, in the ultrafine size range, the operating conditions achievable with a Falcon concentrator cannot benefit from this favourable effect.

3. Concentrated suspensions

The fluid flow assumptions on which the modeling relies have been validated. The model limitations, in terms of par-

ticulate Reynolds number and Stokes number, do not affect its validity to predict the separation of ultrafine particles. Extending the scope of the model to dense suspensions is the last limitation that needs to be overcome in order to obtain a general model of separation with a smooth bowl Falcon concentrator. This has been done using Eulerian tracking of the concentration of each particle class (Kroll-Rabotin et al., 2011a). This method is briefly described hereafter.

3.1. Particle Eulerian tracking model

As the effect of the Stokes number is negligible, particles are always sedimenting at their terminal settling velocity. To account for the presence of other particles, hindered terminal settling velocities are calculated according to the semi-empirical law by Concha and Almendra (1979); Concha et al. (1992). The application of a hindered settling law in numerically solved model for tracking of particle concentration already proved to be satisfactory in the study by Kim and Klima (2004a,b) on hindered settling columns and by Wang et al. (2006) on centrifuge bowls with fluidization at their wall (such as Knelson separators). In order to account for the polydispersity of the treated suspension, the hindered settling model for monodisperse suspensions is applied to each particle class, while concentration effects on the medium sum the effects of all density and size classes (Bürger et al., 2000; Concha and Bürger, 2002).

$$\vec{v}_p - \vec{u}_s = \vec{v}_{\mathrm{C\&A}}\left(r_p, \rho_p, \rho_s, \mu, \omega^2\vec{r}, \sum \phi_p\right) \tag{12a}$$

$$\vec{u}_s = \vec{u} - \frac{\sum \vec{v}_{\mathrm{C\&A,p}}\,\phi_p}{1 - \sum \phi_p} \tag{12b}$$

$$\rho_s = \left(1 - \sum\phi_p\right)\rho_f + \sum\phi_p\rho_p \tag{12c}$$

In this way, terminal settling velocity of each particle can be computed in every point of the flowing film. By discretizing the flowing film in the azimuthal plane, particle concentration in the whole film was computed for each particle class by solving its convection by the particle velocity fields using a finite volume method.

3.2. Concentration fields and particle interactions

Figure 4 shows the concentration fields for different particle classes at different solid concentrations. The feed suspension washability used to plot these graphs is a sample dredged sediment consisting of two phases. The first one is organic with a relative density of 1.292 and the other one is mineral with a relative density of 2.676. Their mass fractions are 11.5% and 88.5%. Their size distributions are modeled by fitted Rosin-Rammler distributions with $d_{63.2} = 12.94\,\mu$m, $k = 0.6369$ for the organic phase and $d_{63.2} = 23.35\,\mu$m, $k = 0.3285$ for the mineral phase respectively. Computations have been run for a Falcon L40 equipped with a smooth UF bowl at a flow rate of 5 l/min, a bowl rotation speed of 1200 rpm and solid concentration in the feed stream of 30 wt.%.

Particle interactions induce several phenomena:

- settling being hindered, particles settle slower and reach the wall bowl later, which leads to a decrease of the recovery to concentrate for any given particle class, provided

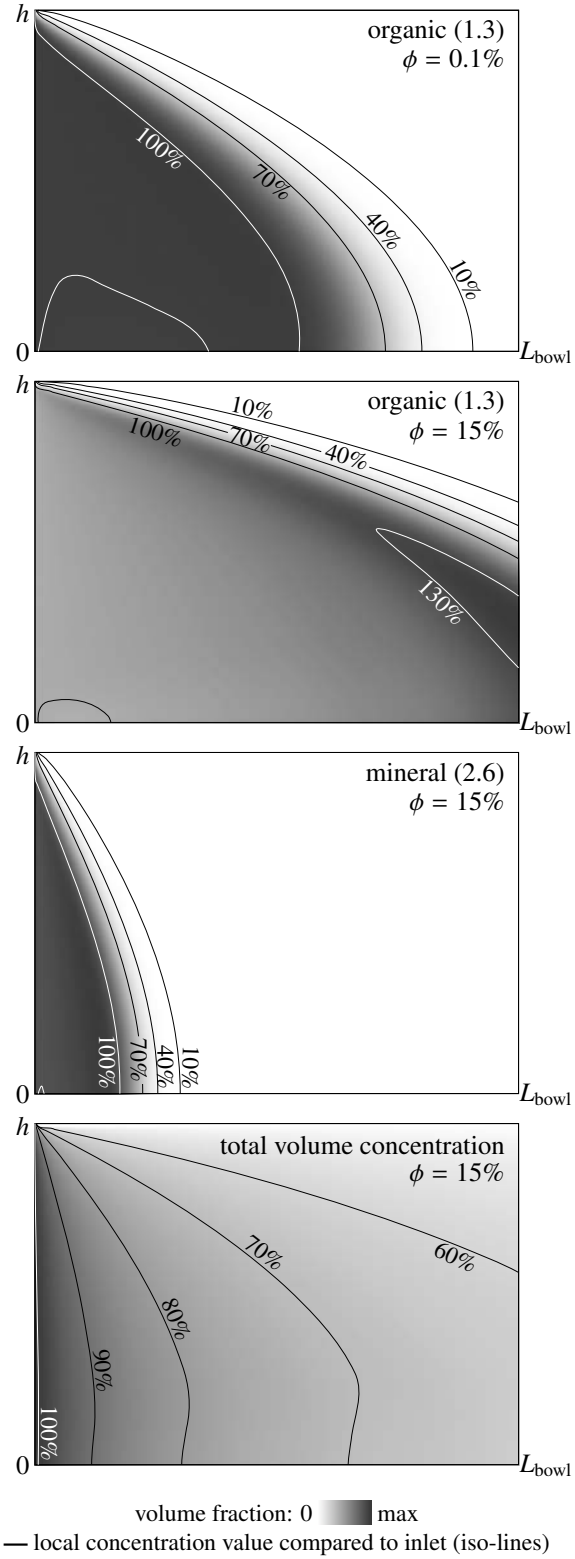

Figure 4: Volume fraction of a 23.5 μm particle from a sample sediment in the flowing film of a Falcon L40 with UF bowl operating at $Q = 5$ l/min and $\omega = 1200$ rpm

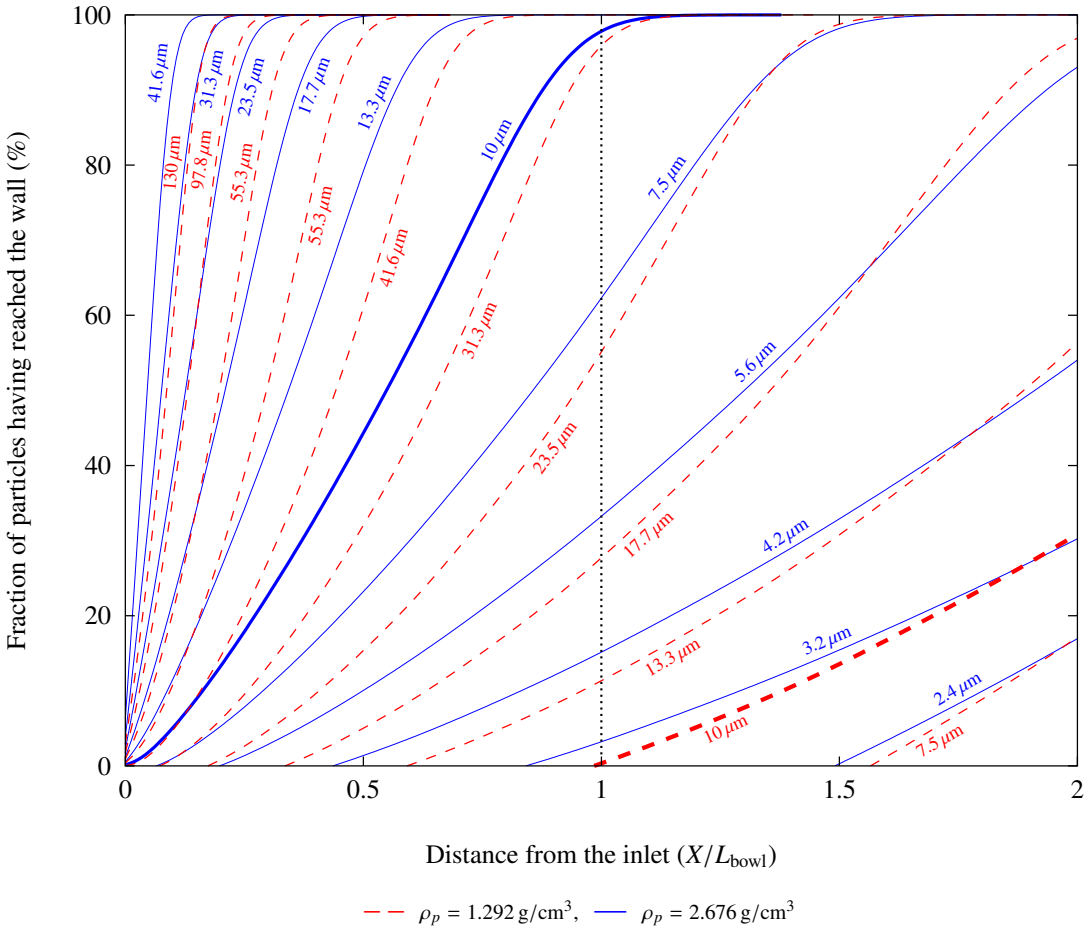

Figure 5: Cumulative distribution onto the bowl wall for each particle class

that all other operating parameters remain constant. This phenomenon appears clearly when comparing the two first graphs in figure 4;

- low density particles are concentrated inside the flowing film before they can reach the wall. As shown in the third graph of figure 4, this is due to the suspension density in the film and to the back flow of dense and coarse particles that settle faster, whose settling creates a fluid flow in the opposite direction for volume conservation. This opposes the settling of lighter and smaller particles. Eventually, for the least dense particles in the suspension, the most concentrated region in a given particle class is not at the inlet but inside the flowing film. Once heavier particles have all settled, lighter particles are able to settle and reach the wall.

For broad size distributions, these effects are noticeable on every particle class, while from a general point of view, the amount of solid in the film always decreases while particles settle and get trapped (cf. last graph in figure 4).

The recovery to concentrate of each particle class is calculated by considering mass fluxes that flow through the boundaries of the inlet, outlet and retention zone. Figure 5 shows how the flux of particles that reach the wall is distributed along the bowl wall, for the same suspension and operating conditions that were used previously. It is easy to visualize the rate of recovery of each particle class by reading the value of the relative cumulative flux at the abscissa corresponding to the bowl length. Some particle classes completely settle before the bowl outlet and are totally recovered (case of particles $\rho_p = 2.676\,\mathrm{g/cm^3}$ and $r_p = 13.3\,\mu\mathrm{m}$), while, due to the local increase of concentration in the film, some particles do not settle at all before the outlet (case of particles $\rho_p = 1.292\,\mathrm{g/cm^3}$ and $r_p = 10\,\mu\mathrm{m}$). For sizes and densities in the vicinity of the cut-point values, the recovery has a value that is neither 0 nor 100% at the abscissa corresponding to the bowl length. Thus, partition function (C_p) can be read as the value of the curves plotted in figure 5 at abscissa 1, for each particle class. In conditions such as the ones used for that plot, density separation is almost perfect for 10 μm particles (bold lines on figure 5).

3.3. *Corrected analytical model*

In order to completely account for both previously identified particle interaction mechanisms, it is necessary to compute the

volume fractions of all particle classes anywhere inside the film. However, for the sake of practical use of the model, it was found that their effect could be modeled in a simpler way by adding two parameters in the analytical model: one of these parameters accounts for the effects of the local density of the suspension, while the other one accounts for the global elongation of the particle trajectories due to hindered settling.

As the resolution of the concentrated problem is done in a completely different way than the previously described dilute one, the application of this model to dilute suspensions does not give the exact same result as the analytical model (1a). The numerical resolution has not been fine tuned so that it converges to the analytical model under dilute conditions. Only the trends from the numerical resolution are needed in order to extend the analytical law. A multiplicative coefficient (of value 0.8) has been included in the analytical expression in order to make the two approaches give the same results in dilute conditions, so that the effect of the physical parameters can be quantified compared to this reference and then be included directly in the handling of concentration effects into the analytical law. Again, it does not hide any physics, as confirmed by the model's fitting to all the trends that have already been described (particle density and size, bowl rotation and flow rates). This correction factor only accounts for the error due to the numerical solution of the model and to the accuracy of its underlying models, and ensures that the asymptotical trend of the numerical simulation matches with the analytical law in dilute conditions. As a result, it should not be included in the extended analytical law, since equation (1a) already fits experimental data. However, for comparisons shown in figures 6, 7 and 8, this factor has been applied to the analytical law as there is no way to add it in the numerical model with certainty that it does not impact the physics.

The effect of suspension density can be modeled using an apparent density in model (1a) that differs from that of the carrier fluid. However, this apparent density is not the suspension density in the feed stream. Indeed, concentration decreases gradually in the film while particles reach the bowl wall and get trapped in the retention zone. Consequently, the density in the feed stream is the maximum value of the apparent density in the whole film, as shown in the last graph in figure 4). Conversely, according to the second graph in figure 4, it appears that low density particles are concentrated before they reach the wall. Thus, they all quickly reach the bowl wall once denser particles have settled and the local suspension density has decreased. Density in the overflow is the last suspension density in the film before the outlet, which means that this is also the last medium density that particles will experience before leaving the bowl. As a result, particles that can settle in these conditions have already settled, while the others are still carried by the film. This critical density is thus the one that must be included in the model. Figure 6 confirms this observation by providing comparisons between density in the tailings and optimal apparent density yielded by fitting analytical model predictions against concentrated medium simulation results.

When increasing the concentration, the distances before impact at the wall of all particle classes increase due to their settling being hindered by particle-particle interactions. This second effect can be modeled by a coefficient that varies with the concentration in the freed stream. This coefficient appears to be a linear function of the volume fraction of the solids, as shown in figure 7 which shows calculated values of this coefficient obtained by minimizing the error of the model predictions, as well as their linear regression. This hindered settling coefficient is then approximately $1 - 1.6\phi$, where ϕ is the volume fraction of the solids in the feed stream.

Equation (1a) becomes:

$$C_p = \min\Big(\frac{4\pi}{9}\,\lambda\,(1-1.6\phi)\; Q^{-1}\,\omega^2\,(\rho_p-\rho_s)\,r_p^2\,\mu^{-1}\,R_{\min}\,R_{\max}\,H_{\text{bowl}}\,,\;1\Big) \quad (13a)$$

where density in the tailings (ρ_s) is calculated this way:

$$\rho_s = \rho_f + \phi \iint (\rho_p - \rho_f)\,(1-C_p)\,f_{\text{feed}}\,\mathrm{d}r_p\,\mathrm{d}\rho_p \quad (13b)$$

Here, C_p and ρ_s are interdependent and an iterative resolution is needed to solve this set of equations. The expression of ρ_s depends on the feed suspension washability (f_{feed}), which meets common understanding that the partition function depends on the washability of the suspension being processed, when the volume fraction (ϕ) becomes non-negligible.

Figure 8 compares separation predictions obtained by solving for the concentrations of all particle classes in the whole film against predictions from the corrected analytical law (13). The results of both approaches are in a very good agreement, which confirms that the two corrective terms that have been added to the analytical law (1a) are sufficient to capture the mechanisms induced by particle interactions that impact the separation. This also means that the physical mechanisms affecting separation are generally the same for both dilute and concentrated conditions, since concentration effect does not change the form of equation (1b) but only adds new factors into it.

Finally, equation set (13) is a very satisfactory separation model for smooth bowl Falcon concentrators. Its predictions can be used to evaluate Falcon's efficiency for processing ultrafine suspensions.

4. Applications to industrial cases

Separation of ultrafine particles is an important challenge in a number of industrial and environmental applications. In this article, we turn our attention to the beneficiation of dredged sediments and fine coal tailings. The former application was in fact the practical problem that supported the work that is presented in the paper.

4.1. Beneficiation of dredged sediments

Every year, millions of tons of sediments are dredged from harbors and various water ways around the globe, hence beneficiation of dredged sediments has become a significant industrial business and a major environmental issue. Dredged sediments

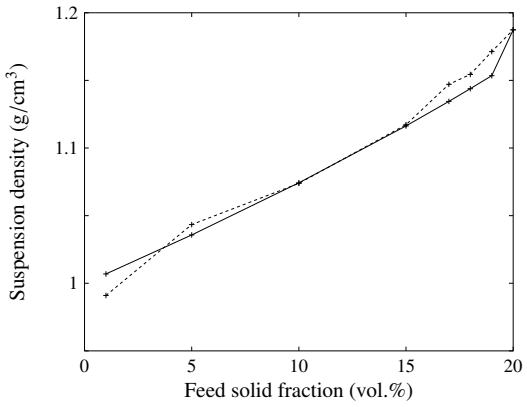

— density in overflow, - - - model fitting
Q = 2 l/min, ω = 1000 tr/min

Figure 6: Comparison between density in overflow and apparent suspension density obtained with least squares method

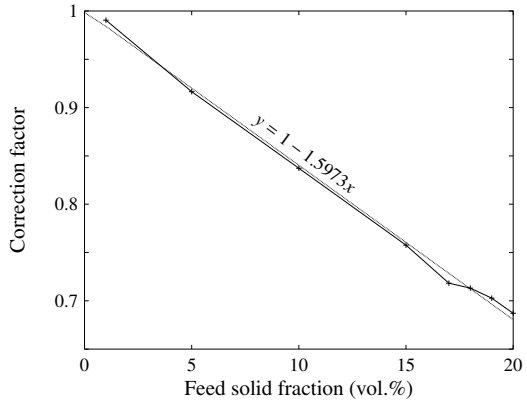

— value of hindered settling coefficient, ··· linear fit
Q = 2 l/min, ω = 1000 tr/min

Figure 7: Least squares calculated correction factor to be included in analytical law to account for separation dependency on feed solid fraction

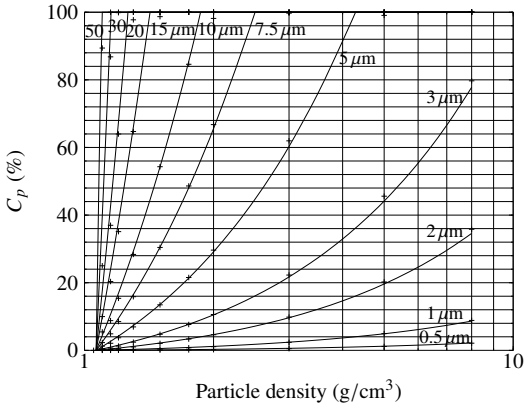

Suspension made of particles ranging in 1.05–8 g/cm^3 and 0.5–50 μm
ϕ = 10%, Q = 3 l/min, ω = 1200 tr/min
— analytical law, + simulation result

Figure 8: Recovery according to particle density: comparison between simulation results and extended analytical law (13)

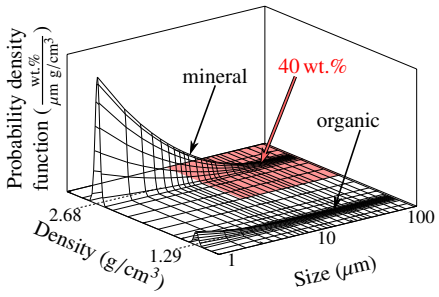

Figure 9: Washability of a sample of dredged sediment

can be considered as a two-phase material of fine sand and organic particles. In many instances, the sand fraction coarser than 10 μm is free of pollutants, which implies that the +10 μm sand fraction can potentially be beneficiated. Unfortunately, current treatment plants are only able to concentrate sand particle larger than 60 to 80 μm with physical separation processes, which may represent only half of the potentially valuable sand particles. Given the tonnages involved, there is a very strong incentive to identify robust technologies for concentrating sand particles from 10 μm upwards. In this size range however, the competing effects of particle size and density are significant, despite the 1.3 s.g. difference between sand and organic particles.

Previous studies (Detzner, 1995) attempted to concentrate dredged sediments using small diameter hydrocyclones. However, this solution suffered from important wear issues and still could not achieve efficient separation below 63 μm. Achieving the desired result implies both a size-based separation above 10 μm and a density-based separation between 2.6 and 1.3 *s.g.* Since our work has shown that the UF Falcon concentrator operates a separation based on both particle size and particle density in this range, it seemed interesting to assess the potential of the UF Falcon for this industrial application by interrogation of our model (13). The washability of the used dredged sediments is given in figure 9.

As shown in equation (1) and detailed in section 2.2, the particle transport regime remains the same for all the conditions at which a Falcon concentrator may operate. Although they weigh differently on separation, the flow rate and the rotation rate can be grouped into a single parameter $Q^{-1}\omega^2$. Equation (13a) confirms that this remains valid under dilute and concentrated conditions. Adjusting both the flow rate and the rotation rate makes it possible to reach a ratio of approximately 250 between the maximum and minimum values of this unique parameter with a Falcon L40. This permits processing a broad range of slurries with the same device.

To simplify the use of this parameter, a reference operating condition set is chosen with Q_0 = 5 l/min and ω_0 = 1200 rpm. The behavior at other operating conditions is then studied relative to this reference, as per the horizontal axis in figure 10.

Different set points were applied to a typical sediment washability whose valuable content, defined here as the sand fraction in the 10 to 150 μm range, is approximately 40% (same as in

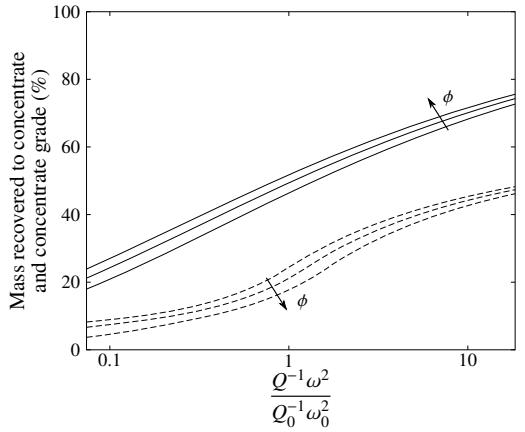

— total mass ratio to concentrate
--- non-valuable content in concentrate (organics and $-10\,\mu$m minerals)
⟶ increasing feed concentration ($\phi = \{0, 21, 38\}$ wt.%)

Figure 10: Impact of operating parameters on separation result for a typical dredged sediment

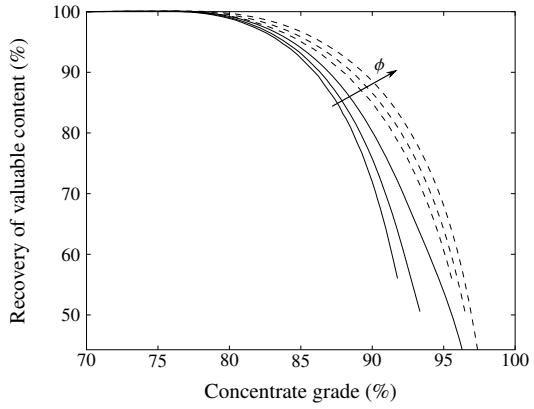

— sample sediment washability (see figure 9)
--- sample sediment washability with finer organic particles
⟶ increasing feed concentration ($\phi = \{0, 21, 38\}$ wt.%)

Figure 11: Grade-recovery curves of different sediment washabilities at different operation conditions

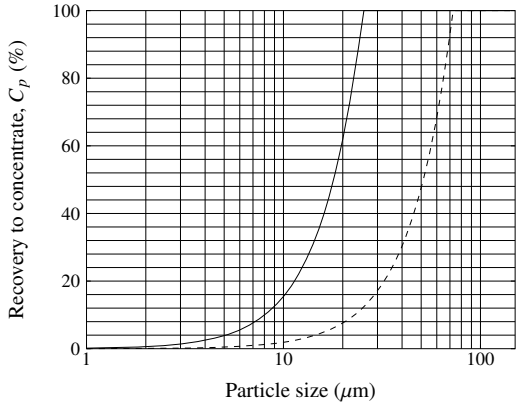

$-\,-\,\rho = 1.29$ g/cm^3, — $\rho = 2.65$ g/cm^3

Figure 12: Predicted partition curves of a sample sediment with a Falcon L40 operating at 0.18 $Q^{-1}\omega^2/(Q_0^{-1}\omega_0^2)$, feed solid fraction being 21 wt.%.

section 3.2, also plotted in figure 9). The performance of the UF Falcon can be investigated by varying the feed solid fraction and the parameter that couples flow and rotation rates which was defined earlier. The results obtained for a Falcon L40 are plotted in figure 10. It shows that even though concentration effects improve separation efficiency, their contribution may be overruled by the flow and rotation rates. This figure shows two quantities that vary with the operating conditions: the mass recovery to concentrate and the amount of non-valuable material in the concentrate. As expected from grade-recovery analysis, both of them increase with $Q^{-1}\omega^2$, which means that the more valuable material is recovered, the more non-valuable material is retained too, since all particles undergo the same physics, though their quantitative response is different.

As expected, figure 10 shows that the lower the recovery, the cleaner the concentrate. The best result is obtained with the combination of high flow rate and slow bowl rotation speed. Even in this case, the concentrate is still around 3.7 % of presumably polluted material, that is minus $10\,\mu$m sand and organic particles. Depending on the nature of the pollution associated with the sediments, such a grade may be acceptable for beneficiation, however it comes at the cost of recovering only 18 % of the total mass, which corresponds to 44 % recovery of the valuable material. This is not sufficient to justify processing such a material in industrial cases, especially because these values rely on a high concentration which is hard to keep constant in industrial processes.

Figure 11 summarizes the data presented in figure 10 (continuous lines) and more in the form of a usual grade-recovery curve. The results show that for a sample dredged sediment, it is hardly possible to obtain a concentrate with less than 5 % of presumably polluted content. This is too high to consider this product as a clean product for any realistic situation, especially as this result is obtained at the best separation conditions and comes at the cost of recovering only half the non-polluted material which would only decrease the final amount of produced waste by 30 %. Figure 12 shows that the separation curves are quite steep. Therefore, Falcon separators produce a really sharp separation. The issue here is that the cut point dependency on particle size does not match what is needed for beneficiating dredged sediments. As the separation limitations mostly arise from the particle size distribution, they cannot be solved by using multiple passes through Falcon concentrators.

Following the results which showed that the UF Falcon is unable to meet the $+10\,\mu$m objective with the natural dredged sediment washability, the next course of action was to investigate whether changing the washability itself might give new scope for beneficiation. This possibility was considered since organic particles were found through experiments to be significantly more sensitive to attrition than sand particles, so that intensive mixing for instance could reduce the size of organic particles selectively. This behavior, which is specific to the material of interest, will increase the particle size differential between sand and organic particles, thereby providing the UF Falcon with more favorable conditions for separation.

The new size distribution of organic particles was modeled using a Rosin-Rammler distribution with $d_{63.2} = 10\,\mu$m and ex-

Table 1: Sample mass distribution of coal fines

mass %	density range (g/cm^3)			
size range (μm)	1.2 – 1.40	1.40 – 1.45	1.45 – 1.50	1.50 – 8.18
100 – 200	4.04	3.06	3.01	4.25
80 – 100	4.29	3.23	3.03	5.09
63 – 80	0.87	0.58	0.51	0.95
40 – 63	5.45	3.41	1.88	3.25
20 – 40	7.33	5.39	2.08	4.52
5 – 20	5.99	6.35	7.97	12.39
0 – 5	0.41	0.00	0.00	0.67

ponent $k = 1$ (cf. 3.2). Analyzing Falcon's ability to treat this new washability using the same method as with plain sediment washability yields significantly better separation efficiency (cf. figure 11). In fact, running at $0.13 Q_0^{-1} \omega_0^2$ gives a concentrate grade of approximately 5% and a recovery between 25 and 30 wt.%. It is observed that the grade does not depend strongly on the concentration of solids in the feed stream anymore. These conditions are far more interesting for industrial applications than the previous ones. The actual benefits that can be expected from such a process will depend on the distribution of the contamination throughout the sediment washability, which will control the sand fraction that can be beneficiated. It is noted that minus 150 μm particles were used in these simulations. Better results can be expected with the Falcon concentrator if it is fed with a narrower size distribution, such as minus 63 and 80 μm, which are achievable cut sizes with industrial dredged sediment treatment plants.

4.2. *Coal fines*

Recovery of coal fines from plant tailings is another industrial process that faces ultrafine particle beneficiation challenges. Falcon concentrator's potential application for this process was evaluated by applying the analytical model (13) to a sample washability of coal fines (cf. table 1 and figure 13) whose grade is around 70%.

To quantify the separation efficiency and to determine conditions at which the Falcon concentrator should be operated in order to concentrate this coal, the following function was mini-

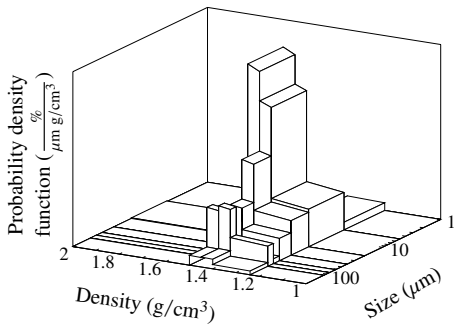

Figure 13: Sample washability of coal fines

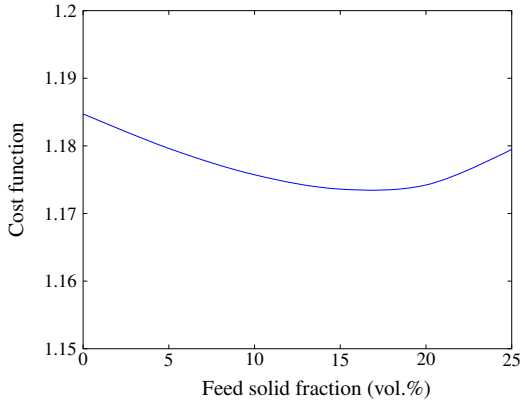

$Q = 15\,$l/min, $\omega = 2400\,$rpm

Figure 14: Search of optimal feed solid concentration for ultrafine coal recovery by minimizing cost function (14)

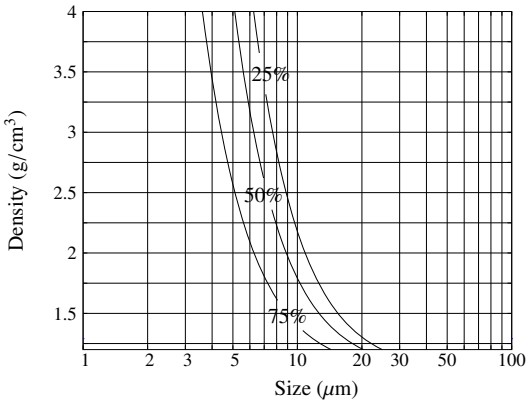

Figure 15: Partition function: recovery to overflow ($1 - C_p$) of sample ultrafine coal at 15 l/min, 2400 rpm and 16 vol.%.

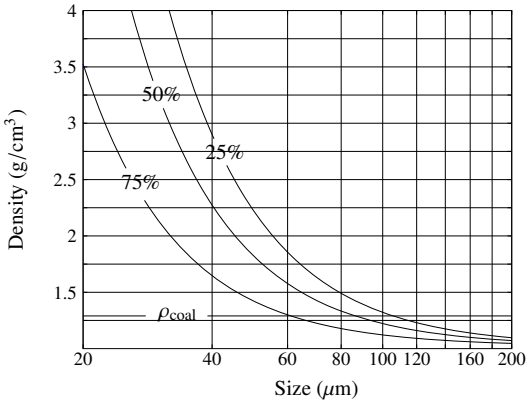

Figure 16: Partition function: recovery to overflow ($1 - C_p$) of coal fines over 45 μm at 30 l/min, 700 rpm and 20 vol.%.

mized:

$$\text{cost}(G_{\text{out}}, C_m) = \sqrt{(K\,(1 - G_{\text{out}}))^2 + (1 - C_m)^2} \tag{14}$$

This cost function involves the concentrate grade (G_{out}) and the mass fraction of recovered solids (C_m) which both are parameters whose values must be as high as possible in order to achieve good separation from an industrial point of view. Initially, the product grade is given a far bigger weight (with $K = 10$), because it is a mandatory condition for industrial markets, while recovery rate is a process optimization. As detailed in section 4.1, there is no such thing as a unique set of optimum operating conditions. Instead, there is a continuous range of bowl rotation rates and corresponding flowrates that perform the same best achievable separation. Operating at such optimal conditions according to this cost function ($Q = 15\,\text{l/min}$, $\omega = 2400\,\text{rpm}$) results in a concentrate grade of 92% and a recovered mass fraction of around 15%. Over the whole range of operating conditions, it does not seem possible to get a product with a significantly higher grade.

Figure 14 shows the effect of the concentration of solids in the feed stream on function (14) while other operating parameters remain constant. It reaches its minimum value for a feed volume fraction $\phi \approx 0.16$ (that is around 25 wt.%). At this feed solid concentration, suspension density in the overflow is still much lower than the density of coal ($1.01\,\text{g/cm}^3$), so the effect of concentration is not expected to significantly improve the separation according to particle densities. What is actually observed here is a shift in the size cut point, which is consistent with the observed grade quality limitation due to the inability to efficiently separate the different phases based on their densities. This is illustrated by figure 15 that shows the partition function at optimal operating conditions. The cut-point line is almost vertical, meaning that the separation is mostly size dependent.

This observation is in good agreement with the analysis of Abela (1997), Bradley et al. (2000) and Honaker et al. (1994–2004). Indeed, they conclude that Falcon concentrators are not able to beneficiate coal below $45\,\mu\text{m}$. To overcome this limitation, some studies focused on improving the density cut-point using a dense medium (Honaker and Patil, 2002; Honaker et al., 2000). Model (13) is able to predict the impact of such a solution through its effect on concentration in the overflow (which is the product in the case of coal while denser tailings are retained in the bowl).

In order to compare model results against conclusions by these authors, size fraction below $45\,\mu\text{m}$ was removed from the previously used washability. Separation predictions for this new washability show a different behavior. In fact, many operating condition sets lead to product grade as high as 100% (some of them come at the cost of a very low recovery rate).

The previously defined cost function is here almost independent from the value of parameter K (for $0 \leq K \leq 10$), which shows that it almost only accounts for the impact on the recovered fraction. With the coarser new washability, this function has no minimum within the operating condition ranges that are reachable with a Falcon L40. It improves monotonically when increasing flow rate, decreasing bowl rotation speed or increasing feed solid fraction. For extreme operating conditions of the Falcon L40 ($Q = 30\,\text{l/min}$, $\omega = 700\,\text{rpm}$ and 30 wt.% feed concentration), the predicted recovery ratio is around 30% for a grade quality of approximately 98%, which confirms that the limitations on concentrating ultrafine coal do not appear for coal that is coarser than $45\,\mu\text{m}$. This is consistent with observations detailed in the literature. Moreover, the authors who studied coal beneficiation with a Falcon concentrator did not necessarily need to operate it under such extreme conditions. Contrary to UF bowls, they were using SB bowl in which they could adjust the recovery rate by varying the fluidization counterpressure. It is thus acceptable that their results are quantitatively different from our results. The important point is the fact that our model is able to predict the patently opposite trends between coal fines and ultrafines.

Figure 16 shows the partition function obtained at such extreme operating conditions with a Falcon L40. The density of clean coal is indicated. From this figure, it appears that, with such conditions, coal is concentrated below $100\,\mu\text{m}$: 25%-recovery curve is equal to clean coal density in the vicinity of $100\,\mu\text{m}$ (coal being less dense than the impurities, the product is the overflowing fraction). This corresponds to the size range targeted by such Falcon concentrators. On the contrary, separation concentrates more and more denser particles that contain more gangue when size decreases. Since these are extreme operating conditions for this device and for the analytical model, it does not make sense to use these results to deduce the critical size below which separation becomes inefficient, especially since this size depends on the washability of the processed suspension. Figure 16 still gives an interesting clue about separation trends.

It might still be possible to overcome this limitation by leveraging fluidization in SB bowls. But, mechanistic models currently lack the ability to account for it. Studies that used fluidization were purely empirical. Although they provide valuable quantitative results, they are not able to draw conclusive interpretation about separation trends that would help define potential improvements to the coal enrichment process. To extend the presented analytical model to other Falcon series, deeper understanding of the fluid flow in the retention zone of Falcon SB and C bowls would be needed.

5. Conclusions

This paper presents a predictive analytical model for ultrafine particle separation with a smooth-bowl Falcon concentrator. This model was developed through a detailed analysis of the physics of this concentrator, on the assumption that the prevailing separation mechanism is particle transport in a flowing film. The model has been successfully validated using a range of experimental and numerical investigations. While the model described here enables more comprehensive interpretation of experimental data, it in fact is an ideal tool with which a more general analysis of the concentrator's intrinsic strengths and limitations could be investigated. This is in sharp contrast to experimental studies (Duan et al., 2009; Oruç et al., 2010), which provide only information on the concentrator's ability to process specific suspensions. This analytical model can also

be used for process investigation or optimization, and two case studies, for dredged sediments and coal fines, were described. This work represents a significant step forward in the simulation of separation processes involving a Falcon concentrator, or any device whose principles of operation are similar.

In the future, it is expected that this model will be extended to the study of continuous discharge concentrators. These are very sensitive to fluctuations in their feed stream due to the low amplitude of concentration variations they can withstand in their discharge valves. Our model is able to relate this concentration to the feed properties and the discharge rate, which would make it possible to relate the feed fluctuations to their impact on the separation.

Appendix A. Time scales

Though physical separators' typical usage is for processing non-reacting slurries, and as such, time scales are of limited interest in these units, two specific time scales can be evaluated: the residence time of particles in the concentrator, and the operating cycle duration.

As particles entering the retention zone are definitely trapped, their residence time is infinite. For the fraction flowing out with the carrying fluid, their slip velocity is negligible compared to the fluid velocity in the streamwise direction. Let Δt be the average residence time of the overflowing particles, then:

$$\begin{aligned}\Delta t &= \frac{L_{bowl}}{u_{mean}} = \frac{L_{bowl}\,\mathcal{A}_{film}}{Q} \\ &= \mathcal{V}_{film}\,Q^{-1} = \pi R^2\,h\,Q^{-1}\end{aligned} \tag{A.1}$$

For a Falcon L40, operating at 15 l/min and spinning at 1500 rpm, Δt is approximately 0.2 s.

The duration of an operating cycle is constrained by the volume content of the retention zone ($\mathcal{V}_{trap} \approx 16$ millilitres). The cycle must be shorter than the time required to fill the retention zone. Let ΔT be the operating cycle duration, it can be estimated by:

$$\Delta T = \frac{\mathcal{V}_{trap}\,k_{pack}}{Q\,C_v} \tag{A.2}$$

where k_{pack} is the packed volume fraction of the solids and C_v is the volume fraction of particles retained in the bed. C_v depends on the partition function and on the volume of the particles in the slurry:

$$C_v = \sum_p C_p\,\mathcal{V}_p \tag{A.3}$$

Both k_{pack} and C_v vary from one slurry to another and are easier to get experimentally. When running experiments with silica sand (D50 = 8 μm), critical operating cycle duration was of the order of a few minutes when retaining about half of the solids.

Appendix B. Nomenclature

Modeling of the particle dynamics

λ : calibration constant
P : flow profile
u : fluid velocity
v : particle velocity
G : gravity acceleration
C_D : drag coefficient

Operating conditions

Q : flow rate
ω : rotation rate of the bowl
C_p : partition (or cut) function
C_m : mass ratio to product
C_v : volume ratio to product
f : washability (size and density distribution of particles, by volume)

Physical quantities of the fluid and the solids

r_p : radius of the particle class "p"
ϕ_p : volume fraction of particle class "p"
ρ_p : density of the particles
ρ_f : density of the carrying fluid
ρ_s : density of the mixture
μ : viscosity of the carrying fluid
ν : kinematic viscosity ($= \mu/\rho_f$)

Geometry and coordinates

h : film thickness
r : distance to the bowl's axis of rotation
R : radius of the bowl
H : height of the bowl
β : opening angle of the bowl
X : streamwise direction
Y : wall normal direction
θ : azimuthal direction

Dimensionless parameters

Re_p : particulate Reynolds number
Ar : Archimedes number
Ek : Ekman number

Acknowledgments

This work is funded by the French "Agence Nationale pour la Recherche" (ANR), in the framework of the PROPSED project.

References

Abela, R. L., 1997. Centrifugal concentrators in gold recovery and coal processing. In: Extraction Metallurgy Africa.

Bradley, P., Patil, D. P., Ho, K., 2000. Development and demonstration of an enhanced gravity separator for coal cleaning. Tech. rep., Illinois Clean Coal Institute.

Bruin, S., 1969. Velocity distributions in a liquid film flowing over a rotating conical surface. Chemical Engineering Science 24, 1647–1654.

Bürger, R., Concha, F., Fjelde, K.-K., Hvistendahl Karlsen, K., 2000. Numerical simulation of the settling of polydisperse suspensions of spheres. Powder Technology 113, 77–318.

Concha, F., Almendra, E. R., 1979. Settling velocities of particulate systems, 2. settling velocities of suspensions of spherical particles. International Journal of Mineral Processing 6, 31–41.

Concha, F., Bürger, R., 2002. A century of research in sedimentation and thickening. Kona: powder and particle journal 20, 38–69.

Concha, F., Lee, C. H., Austin, L. G., 1992. Settling velocities of particulate systems, 8. batch sedimentation of polydispersed suspensions of spheres. International Journal of Mineral Processing 35 (3-4), 159–175.

Coulter, T., Subasinghe, G. K. N., 2005. A mechanistic approach to modelling Knelson concentrators. Minerals Engineering 18, 9–17.

Detzner, H. D., 1995. The Hamburg Project METHA: Large scale separation, dewatering and reuse of polluted sediments. European Water Pollution Control 6 (5), 38–42.

Deveau, C., 2006. Improving fine particle gravity recovery through equipment behavior modification. In: 38th Annual Meeting of the Canadian Mineral Processors. Paper 31. pp. 501–517.

Dijk, P. E., Janse, A. M. C., Kuipers, J. A. M., van Swaaij, W. P. M., 2001. Hydrodynamics of liquid flow in a rotating cone. International Journal of Numerical Methods for Heat & Fluid Flow 11 (5), 386–412.

Duan, C., Wen, X., Shi, C., Zhao, Y., Wen, B., He, Y., 2009. Recovery of metals from waste printed circuit boards by a mechanical method using a water medium. Journal of Hazardous Materials 166, 478–482.

Holtham, P., Gee, B., Dunne, R., Gregory, S., 2005. Recovery of fine gold particles using a Falcon 'B' separator. In: Deschenes, G. (Ed.), International Symposium for the Treatment of Gold Ores.

Honaker, R. Q., Das, A., 2004. Ultrafine coal cleaning using a centrifugal fluidized-bed separator. Coal Preparation 24 (1–2), 1–18.

Honaker, R. Q., Patil, D. P., 2002. Parametric evaluation of a dense-medium process using an enhanced gravity separator. Coal Preparation 22 (1), 1–17.

Honaker, R. Q., Paul, B. C., Wang, D., Ho., K., 1995. Enhanced gravity separation: an alternative to flotation. In: Society for Mining, Metallurgy and Exploration Annual Meeting. High Efficiency Coal Preparation: An International Symposium.

Honaker, R. Q., Paul, B. C., Wang, D., Huang, M., 1994. Application of centrifugal washing for fine coal cleaning. In: Society for Mining, Metallurgy and Exploration Annual Meeting.

Honaker, R. Q., Reed, S., 1995. A fine coal circuitry study using column flotation and gravity separation. Tech. rep., Department of Energy.

Honaker, R. Q., Singh, N., Govindarajan, B., 2000. Application of dense-medium in an enhanced gravity separator for fine coal cleaning. Minerals Engineering 13 (4), 415–427.

Honaker, R. Q., Wang, D., 1998. Falcon concentrators: a high capacity fine coal cleaning technology. In: Society for Mining, Metallurgy and Exploration Annual Meeting.

Honaker, R. Q., Wang, D., Ho, K., 1996. Application of the Falcon concentrator for fine coal cleaning. Minerals Engineering 9 (11), 1143–1156.

Janse, A. M. C., Biesheuvel, P. M., Prins, W., van Swaaij, W. P. M., 2000. Granular flow in a rotating cone partly submerged in a fluidized bed. American Institute of Chemical Engineers Journal 46 (3), 499–508.

Kim, B. H., Klima, M. S., 2004a. Development and application of a dynamic model for hindered-settling column separations. Minerals Engineering 17, 403–410.

Kim, B. H., Klima, M. S., 2004b. Simulation of hindered-settling column separations when processing fine anthracite refuse. Coal Preparation 24, 261–275.

Kroll-Rabotin, J.-S., 2010. Analyse physique et modélisation de la séparation centrifuge de particules ultrafines en film fluant: Application au séparateur industriel Falcon. Ph.D. thesis, Institut National Polytechnique de Toulouse.

Kroll-Rabotin, J.-S., Bourgeois, F., Climent, E., 2010. Fluid dynamics based modelling of the Falcon concentrator for beneficiation of ultrafine particles. Minerals Engineering 23 (4), 313–320, special Issue: Physical Separation.

Kroll-Rabotin, J.-S., Bourgeois, F., Climent, E., 2011a. Beneficiation of concentrated ultrafine suspensions with a Falcon UF concentrator. CIM Journal 2 (4), 189–199.

Kroll-Rabotin, J.-S., Bourgeois, F., Climent, E., 2011b. Experimental validation of a fluid dynamics based model of the UF Falcon concentrator in the ultrafine range. Separation and Purification Technology 92, 129–135.

Langrish, T. A. G., Makarytchev, S. V., Fletcher, D. F., Prince, R. G. H., 2003. Progress in understanding the physical processes inside spinning cone columns. Chemical Engineering Research & Design 81 (1), 122–130.

Laplante, A. R., Buonvino, M., Veltmeyer, A., Robitaille, J., Naud, G., 1994. A study of the Falcon concentrator. Canadian Metallurgical Quarterly 33 (4), 279–288.

Laplante, A. R., Nickoletopoulos, N., 1997. Validation of a Falcon model with a synthetic ore. Canadian Metallurgical Quarterly 36 (1), 7–13.

Laplante, A. R., Shu, Y., 1993. A comparative study of two centrifugal concentrators. In: 25th Annual Meeting of the Canadian Minerals Processors. Paper 5. pp. 18–36.

Makarytchev, S. V., Langrish, T. A. G., Prince, R. G. H., 1998. Structure and regimes of liquid film flow in spinning cone columns. Chemical Engineering Science 53 (8), 1541–1550.

Makarytchev, S. V., Xue, E., Langrish, T. A. G., Prince, R. G. H., 1997. On modelling fluid flow over a rotating conical surface. Chemical Engineering Science 52, 1055–1057.

McAlister, S. A., Armstrong, K. C., 1998. Development of the Falcon concentrator. In: Society for Mining, Metallurgy and Exploration Annual Meeting.

Oruç, F., Özgen, S., Sabah, E., 2010. An enhanced gravity method to recover ultra-fine coal from tailings: Falcon concentrator. Fuel 89, 2433–2437.

Schiller, L., Naumann, Z., 1935. A drag coefficient correlation. Zeitschrift des Vereines Deutscher Ingenieure, 77–318.

Wang, X., Miles, N. J., Kingman, S., 2006. Numerical study of centrifugal fluidized bed separation. Minerals Engineering 19, 1109–1114.

Zhao, Y.-M., Wen, X.-F., Shi, H.-X., Jiao, H.-G., Tao, Y.-J., 2006. Study on metals recovery from -0.074 *mm* printed circuit boards by enhanced gravity separation. The Chinese Journal of Process Engineering 6 (2), 201–204.